Title

A structural coarse-grained model for clays using simple iterative Boltzmann inversion

Journal

The Journal of Chemical Physics, 148(22)

ISSN

0021-9606

Authors

Schaettle, Karl

Pestana, Luis Ruiz

Head-Gordon, Teresa

et al.

Publication Date

2018-06-14

DOI

10.1063/1.5011817

Peer reviewed

A Structural Coarse-Grained Model For Clays Using Simple Iterative Boltzmann Inversion

Karl Schaettle[1], Luis Ruiz Pestana[5], Teresa Head-Gordon[1-3,5*], Laura Nielsen Lammers[4,6*]

[1]Department of Chemical and Biomolecular Engineering, [2]Department of Chemistry, [3]Department of Bioengineering, [4]Department of Environmental Science, Policy, and Management

University of California, Berkeley

[5]Chemical Sciences Division and [6]Earth and Environmental Science Area

Lawrence Berkeley National Laboratory

Berkeley, California 94720

Cesium-137 is a major byproduct of nuclear energy generation, and is environmentally threatening due to its long half-life and affinity for naturally occurring micaceous clays. Recent experimental observations of illite and phlogopite mica indicate that Cs^+ is capable of exchanging with K^+ bound in the anhydrous interlayers of layered silicates, forming sharp exchange fronts that lead to interstratification (phase separated) Cs- and K-illite. We present here a clay coarse-grain (ClayCG) model using Iterative Boltzmann Inversion of the all-atom ClayFF model, which we develop first for an anhydrous illite clay, that reproduces features of a previously proposed feedback mechanism of ion exchange. The ClayCG model represents a 70-fold speedup over all-atom classical force fields of clay systems, and predicts interlayer expansion for K-illite near ion exchange fronts. Contrary to the longstanding theory that ion exchange in a neighboring layer increases the binding of K in lattice counterion sites leading to interstratification, we find that the presence of neighboring exchanged layers leads to short-range structural relaxations that increase basal spacing and decrease cohesion of the neighboring K-illite layers. We also provide evidence that the formation of alternating Cs- and K-illite interlayers (i.e. ordered interstratification) is both thermodynamically and mechanically favorable compared to exchange in adjacent interlayers.

***corresponding authors**

Introduction

The environmental impact of cesium adsorption and diffusion into various types of naturally occurring layered silicates has received renewed interest in recent year, especially in the aftermath of the Fukushima Daiichi Nuclear disaster.[1-3] One of the most environmentally threatening products of nuclear fission is Cesium-137, both because of its relatively long half-life (30.2 years) and its affinity for mineral surfaces, which prevents it from leaching from surface soils.[4-5] Cesium is strongly and irreversibly adsorbed to various clay surfaces in the presence of other ions, and can slowly diffuse into the bulk volume of both anhydrous and hydrated layered silicates. [6-8] Due to its intermediate half-life and its relative abundance as a nuclear decay product, Cesium-137 can contaminate environmental sites with dangerous levels of radiation for decades, while most other fallout isotopes may only present a threat on the order of months or years. [9]

Cesium diffuses deep into naturally occurring clays and displaces other types of ions normally found in the interlayer, such as potassium, sodium, and calcium. Because of its ability to selectively exchange radiocesium, illite and similar clays have been investigated for the possibility of remediating radioactive plumes of cesium. [10] Despite extensive experimental study of ion adsorption at the frayed clay edge and exchange of ions in the clay interlayer[7-8, 11-13], the exact mechanism of cesium uptake remains elusive.[14] It is especially unclear how cesium displaces potassium within the interlayer far from the edge in anhydrous interlayers for clays such as illite[11, 15-17]. Some groups have suggested that only hydrated ions within the interlayer or near a clay edge should be capable of exchange[18]; however, this exchange mechanism is very thermodynamically unfavorable in bulk illite, since both potassium and cesium strongly favor anhydrous interlayers.[19] Moreover, cesium is found to have a strong affinity for the weathered clay edge, further suggesting that interlayer hydration is likely not a necessary step either for cesium binding or penetration into the interlayer. [14, 20-24]

Recent experimental[7-8] and computational work[25] supports the direct exchange by diffusion for large ions in the interlayer of several clay types without repeated hydration and dehydration at the edge sites. Instead, cesium has been hypothesized to first bind to frayed clay edges, and then more slowly exchange with the potassium naturally found in the interlayer through a diffusive mechanism.[17, 26] Once potassium begins exchanging for cesium at the weathered edge, it has been proposed that there is a thermodynamic and kinetic driving force to displace additional potassium ions, resulting in an accelerated replacement of potassium ions for cesium.[27] Despite this proposed feed-forward mechanism, it has been observed that the rates of ion exchange over moderate

timescales in neighboring interlayers can vary drastically, and thus suggest that the interlayer ion species becomes stratified.[7-8] Although some thermodynamic arguments have been proposed to explain the stability of interstratified clay particles in other clay types[28-30], the physical reason for the disparity in neighboring interlayer exchange rates in illite is still not entirely clear.

In order to adequately predict the ability of micaceous minerals both to uptake radioactive cesium and its susceptibility to remobilization, it is necessary to understand and model the mechanisms that drive the adsorption and exchange of various ionic species in, for example, anhydrous illite. Recent computational work from our group using the classical ClayFF force field and density functional theory (DFT) has indicated that the presence of cesium ions within potassium interlayers creates mechanical forces that significantly increase the interlayer spacing.[25] This expansion in turn results in lower rate coefficients for ion exchange by 6 to 10 orders of magnitude which accelerates the diffusion of potassium ions.[25] However, the problem of characterizing interstratified particles by definition requires the evaluation of kinetic barriers involving multiple interlayers. Probing the energy landscape of large atomistic simulations of this type is computationally expensive, and motivates the development of a coarse-grain (CG) model that is capable of reproducing the energy barriers to ion diffusion near an exchange front and in interstratified clay particles.

Previous CG simulations of clay include both continuous and discrete models of the clay interlayer[31-34]. In one study, Marry et al. investigated a montmorillonite system with a hydrated interlayer.[31] Their CG model consisted of two uniformly charged plates representing the clay layers held a fixed distance apart. Water was modeled implicitly, and both cations and anions in solution were modeled continuously as an effective density that was allowed to vary over space. This model accounted for the excluded volume of the ions using the mean spherical approximation, an advance on previous continuous models of hydrated clay systems. Using classical density functional theory, the grand potential was minimized to derive the density of ions as a function of distance from the clay surface for sodium ions. These types of CG models can be highly accurate for the calculation of continuous properties such as tensile strength or average interlayer spacing. Several groups have also successfully modelled clay and clay-polymer systems by coarse-graining entire clay layers into one single particle.[35-37] However, continuous, ultra coarse-grained models are fundamentally incapable of capturing site-specific effects such as ion binding, and due to mean-field approximations, would not be expected to reproduce the observed variation in the ion binding energy landscape in anhydrous clay[25].

Other groups have developed more detailed coarse-grain clay models that map multiple atoms to single pseudo-atoms, a common coarse-graining technique.[38] In the model of clay-polymer composites developed by the Coveney group, each montmorillonite clay layer is represented by bonded pseudo-atoms corresponding to ion binding sites.[39-40] The pseudo-atoms in the Suter et al. model are bonded with harmonic potentials derived from an iterative Boltzmann inversion (IBI) of the corresponding all-atom RDFs, and represents the three sheets of the clay layer as a single layer of coarse-grain sites[27]. Many of the coarse-grain potentials of ion-sheet interactions in this model were derived using PMF matching with fixed sheets, and the various coarse-grain potentials were converged sequentially[27]. When deriving the potential between free ions and the bulk sites on the clay sheet, Suter and co-workers used the layer-averaged z-coordinate. This method faithfully reproduced the behavior of ions in the fluidized system, but would likely not be sufficiently accurate for reproducing the behavior of confined ions, which is strongly influenced by charge localization.

Simulations with both DFT and ClayFF indicate that ions in the anhydrous illite interlayer approach interlayer-facing oxygen atoms extremely closely, suggesting that compensatory compression of the neighboring sheets could play an important role in determining the energy landscape.[25] In addition, potassium and cesium ions at equilibrium within the interlayer are tightly confined within ditrigonal coordination cavities with oxygen, with interatomic distances of roughly 3.0 – 3.4 Å.[7, 19] Due to this extreme confinement and the detailed structure of ion binding sites, representing an anhydrous clay layer by a single sheet of coarse-grain sites would likely eliminate important stiff stretching and bending degrees of freedom for determining the energetics of ion diffusion.

We present a coarse-grain model of an anhydrous illite clay system with different coarse grain types for representing both the tetrahedral and octahedral sheets that attempts to overcome some of these previous limitations, and derived through IBI using structural information from ClayFF. Our ClayCG model runs approximately 70 times faster than the all-atom implementation in ClayFF within the LAMMPS[41] simulation environment due to both reduced number of interaction sites as well as permitting much larger timesteps of up to 10 fs for molecular dynamics simulations. Hence while ClayFF is typically used to study only a few layers, our ClayCG model is capable of investigating large systems (10^{-6} m) on simulation timescales of microseconds, and the model is available to others through the LAMMPS simulation package. We show that the representation of a much larger numbers of clay layers is necessary to completely eliminate finite size effects in the determination of converged diffusion barriers, and allowing us to provide evidence of a

thermodynamic compensation mechanism for interstratification of potassium and cesium ion distributions in anhydrous illite clay interlayers.

Methods

Simulation cell setup. Classical molecular dynamics (MD) simulations of an atomistic 2-layer illite clay under periodic boundary conditions were used as a reference for generating a coarse-grain (CG) model using iterative Boltzmann inversion. The all-atom MD simulations were performed using the ClayFF[42] forcefield within the LAMMPS[41] simulation package. The ClayFF forcefield is a generalized, nonbonded model for hydrated clays, and consists mainly of Lennard-Jones and electrostatic interactions between atomic centers for bulk clay. It has been fitted to multiple multi-sheet, aluminosilicate clay types including kaolinite ($Al_2Si_2O_5(OH)_4$) and pyrophyllite ($AlSi_2O_5(OH)$), and has been shown to reproduce the swelling behavior of montmorillonite ($Na_3(Si_{31}Al)(Al_{14}Mg_2)O_{80}(OH)_{16}$) very accurately.[42] In addition, ClayFF has been used extensively to study the dynamics of ion adsorption in hydrated interlayers.[43-45] Because of its ability to model multi-layered clay systems under a variety of physical conditions, ClayFF was chosen as the reference atomistic forcefield for our coarse-grain model, and hence the resulting ClayCG model will inherent all of the strengths and limitations of the parent all-atom force field.

All-atom molecular dynamics simulations were run at 300 Kelvin for 100 picoseconds with a timestep of 1 fs after an initial equilibration period of 120 picoseconds. Coordinates of all atoms were sampled every 250 fs to build an ensemble for using the IBI algorithm. Each coarse-grain simulation was sampled in the NVT ensemble for 40 picoseconds after an equilibration of 100 picoseconds with a timestep of 3 fs to compromise between fast turnaround time and sufficient sampling for IBI. To ensure faithful reproduction of the all-atom data, the coarse-grained systems used during the IBI procedure were mapped directly from the corresponding all-atom systems.

CINEB calculations. Climbing-Image Nudged Elastic Band (CINEB)[46-48] calculations were performed using the "neb" command within LAMMPS to obtain energy barriers for interlayer counterion (K^+ and Cs^+) migration, using 25 images integrated with a 5 femtosecond timestep. Before beginning each NEB calculation, both ion position and substitution sites were randomized. The first image for each NEB calculation was generated by equilibrating the randomized structure, and the final image had one ion from the first image displaced to an empty binding site. The remaining images were generated by linear interpolation of the ion position, so that the ion's initial trajectory was a linear path between an occupied and unoccupied site. Oxygen atoms surrounding

the initial and final ion binding sites were included in the reaction coordinate due to their displacement during ion diffusion. By including these atoms in the reaction coordinate, the distribution of energy barriers was reduced by around 30% without significantly altering the mean diffusion barrier value, indicating that this accurately captures important physical effects.

To determine system enthalpies, five-interlayer clay systems with different patterns of ion interstratification, periodic in the x- and y-directions with dimensions of 93 Å and 60 Å, respectively, were relaxed in the non-periodic z-direction over a period of 150 ps using a 3 fs timestep. The z-direction was non-periodic, and was initialized at 50 Å. The simulations were integrated using the multilevel summation method (MSM) real-space electrostatics.[49-50] This electrostatic integration method computes short-range interactions exactly, and computes long-range interactions by decomposing the potential into a sum of smooth potentials which are integrated with a series of progressively coarser meshes. MSM has a competitive level of accuracy as PME for calculating long-range electrostatic interactions, and unlike PME can be used for non-periodic systems. Using the "shrink-wrap" feature in LAMMPS[41], the z-dimension of the simulation box was allowed to dynamically change over the course of each simulation until convergence. This procedure resulted in the system reaching the interlayer spacing that minimized the system enthalpy.

ClayCG model parametrization. The iterative Boltzmann inversion (IBI) algorithm for coarse-graining attempts to reproduce all-atom pair correlation functions by constructing a pairwise interaction potential, a consequence of Henderson's uniqueness theorem.[51-52] CG simulations are run iteratively, and the new pair correlation function $g_{CG}(r)$ is used to update the old interaction potential. Assuming only pairwise effects, the all-atom pair correlation function $g_A(r)$ of gases can be roughly approximated:

$$g_A(r) \approx A\, e^{-\beta u(r)} \tag{1}$$

where A is an arbitrary constant, β is the thermodynamic beta, and $u(r)$ is the potential as a function of the radial separation. The iterative Boltzmann inversion algorithm updates the coarse-grain potential based on the all-atom and CG pair correlation functions:

$$u_{CG,n+1}(r) = u_{CG,n}(r) + \frac{1}{\beta}\left(\ln\left(\frac{g_{CG}(r)}{g_A(r)}\right)\right) \tag{2}$$

Henderson's uniqueness theorem is only precisely true for a homogenous fluid, but IBI is a robust method of coarse-graining that works for heterogeneous fluids and other phases as well. In particular, good performance of the IBI algorithm can be expected if run simultaneously for "orthogonal" degrees of freedom, such as the inter- and intra-sheet forces in our ClayCG model of illite. The iterative Boltzmann inversion procedure was interfaced with LAMMPS by updating non-bonded and bonded coefficients as well as tabulated potentials after each iteration.

The ClayCG model of anhydrous clay consists of 5 different coarse-grain centers. This mapping reduces the number of tracked centers in ClayFF by approximately 2:1 for the bulk clay. The five ClayCG centers are as follows: 1 CG type for the octahedral sheet (Type Al) corresponding to the structural Al^{3+} cations; 2 CG types for the tetrahedral sheet, representing O^{2-} anions directly adjacent to the interlayer, but are separated into CG types corresponding to oxygen anions near sites with and without isomorphic substitutions of Al^{3+} for Si^{4+} (Type Os and O), so that their interactions with other CG centers are computed separately in order to capture differences in the binding site characteristics. In addition, there are two types of ions (Type K and Cs). Silicon and aluminum are not explicitly tracked in the tetrahedral sheet.

The ClayCG sites experience five types of forces based on the following interaction potential: harmonic bonds and angles between neighboring centers in the octahedral and tetrahedral sheets, Lennard-Jones interactions between CG centers, electrostatics between ion and substituted-oxygen CG centers, and finally tabulated forces (Eq. (3)).

$$U = \sum_{bonds} k_b \left(r - r_0\right)^2 + \sum_{angles} k_a \left(\theta - \theta_0\right)^2 + \sum_{LJ} 4\epsilon \left(\left(\frac{\sigma}{r}\right)^{12} - \left(\frac{\sigma}{r}\right)^{6}\right) + \sum_{i} U_{tab,i.}\left(r\right) + U_{electrostatic} \qquad (3)$$

The Lennard-Jones interactions are defined between each pair of CG centers, and are not based on mixing rules; this approach was chosen because the CG centers represent different numbers of atoms from the all-atom model, and therefore the pairwise interactions are unlikely to be characterized by effective radii. Lennard-Jones interactions are slightly less computationally expensive than tabulated forces, and are sufficient for the purposes of this study for characterizing the forces between sheets. Tabulated potentials are used between the ion and tetrahedral CG centers to more accurately capture the nature of the binding sites. Lennard-Jones interactions and electrostatics are excluded for 2nd, 3rd, and 4th neighbors based on the bond and angle topology. After each round of IBI, the updated ClayCG potential is fitted to either a harmonic or Lennard-Jones function for most of the degrees of freedom, and this fit is used in the next round of MD simulation.

In some cases, the same parameters were used to characterize multiple interactions due to the corresponding all-atom model centers having very similar pair correlation functions. For example, one single Lennard-Jones potential was used to govern the nonbonded interaction between the octahedral and tetrahedral CG sites. This approach further simplifies the model, although it does not affect its computational cost. To run our CG clay model, all that is needed is a properly configured input script and data file with the clay system coordinates, charges, and topology. No modification to the LAMMPS software itself is needed to run the model, and the software used to run the IBI algorithm is entirely separate from the core codebase of any simulation software. The CG model is highly portable, and should be able to run on any other molecular simulation package that allows for the implementation of tabulated potentials.

Results

ClayCG performance. Figures 1 and S1 show the distribution of bond distances and angles for the all-atom and ClayCG models for the degrees of freedom fit with harmonic bonds, in which we observe overall excellent agreement. For the non-bonded degrees of freedom, Figures 2 and S2 present the radial distribution function (RDF) of the all-atom model in comparison to the most converged iteration for the ClayCG model. Since the fit for the nonbonded degrees of freedom to the Lennard-Jones functions used only the first peak of each rdf, there is a relatively good agreement for all pair correlations with the exception of the O-O and O-Al CG types. However, even in these cases there is relatively good reproduction of the positions of secondary peaks in the RDFs, indicating that the geometry of the ClayFF and ClayCG systems are quite similar. The model is well converged based on the similarity of the oxygen-ion CG center RDF to the corresponding distribution in the all-atom ClayFF model, since these degrees of freedom are the most important for fully characterizing the ion binding site.

In order to quantify the increase in speed for our coarse-grain model, the all-atom ClayFF model and the corresponding ClayCG model were run for 3 nanoseconds on 32 cores, and the real time needed to simulate each 100 fs was recorded. The all-atom system consisted of 2 clay layers with periodic boundary conditions and a total of 9099 atoms. The ClayCG model ran roughly 6.9 times faster than the corresponding all-atom model with the same timestep. The shortest vibrational period in the all-atom model is on the order of 10 fs due to the explicit modeling of hydrogen[53], and in contrast the fastest vibrational mode in the coarse-grain model presented here is between oxygen-oxygen centers, which is on the order of 100 fs.[53] Because of this, the ClayCG model is stable with a

timestep of up to 10 fs, while ClayFF must use an integration timestep on the order of 1 fs. Thus our ClayCG model represents a roughly 70-fold speedup compared to the corresponding all-atom forcefield, which is comparable to the speedup obtained by other groups using similar coarse-graining techniques.[39-40]

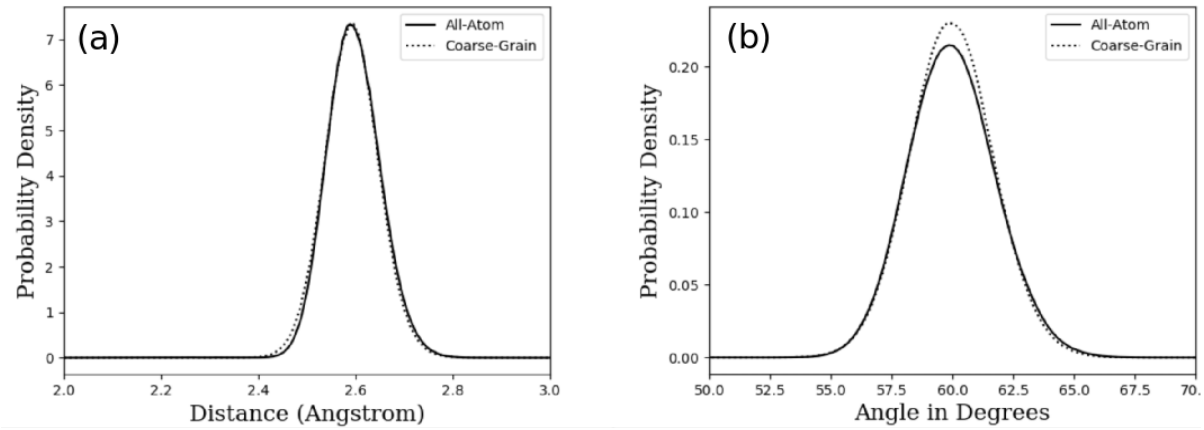

Figure 1. *Comparison of the probability distribution of bond distances and bond angles for the ClayFF (solid) and ClayCG model (dotted)*. (a) Distribution of bond distances for the O-O CG bond; (b) Distribution of bond angles for the O-O-O 60 degree angle type bond.

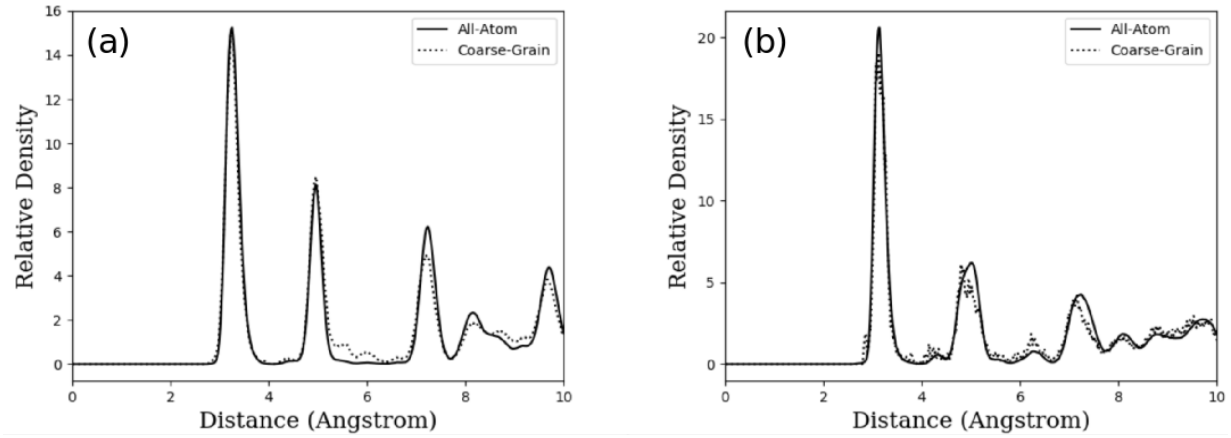

Figure 2. *Comparison of the radial distribution function (RDF) for the ClayFF (solid) and ClayCG model (dotted).* RDFs for (a) O-Cs CG types and (b) Os-Cs CG types. RDFs were sampled every 250 fs over a time period of 40 ps in equilibrated systems.

As shown by Johnson et al., the Henderson uniqueness proof implies that there is always a representability problem as a general feature of a CG potential, i.e. a CG procedure cannot simultaneously resolve all the properties at a given state point.[54] For example, reproducing the energetics of a system when the coarse-graining approach is based on reproducing structural or geometric features of the more complex reference system is not formally guaranteed.[20, 55] However,

the structural coarse-graining approach is likely to reproduce *qualitative* trends in properties such as energetic barriers for ion diffusion in anhydrous clays, since these barriers will be primarily determined by mechanical forces.

Energy barriers to ion migration in pure phases

We sought to further validate our ClayCG model by performing NEB calculations to determine diffusion barriers for different ions in the presence of the same or different ions in the clay interlayers. The mean energy barrier for the migration of potassium in pure K-illite was found to be 300 ± 94 kJ/mol (Figure 3a) on average, compared to 226 ± 51 kJ/mol in the corresponding ClayFF model (Figure 3b). We also found for both K^+ and Cs^+, the energy barrier for diffusion was found to be much lower in systems with a higher fraction of Cs^+ atoms in the interlayer. This result is in agreement with the trend derived from the all-atom forcefield, which has led to our determination of a mechanism for interlayer exchange[25], whereby as more Cs^+ enters an interlayer, both ion species become much more mobile, effectively increasing the rate at which the exchange front will advance into the interlayer.[7-8, 27] While the energy barriers derived from the coarse-grain model were consistently higher and had a broader distribution than the corresponding barriers in the all-atom ClayFF model, these results confirms that the ClayCG model qualitatively reproduces the trends in diffusion energy barriers for K^+ and Cs^+ found previously in the all-atom clay model.[25]

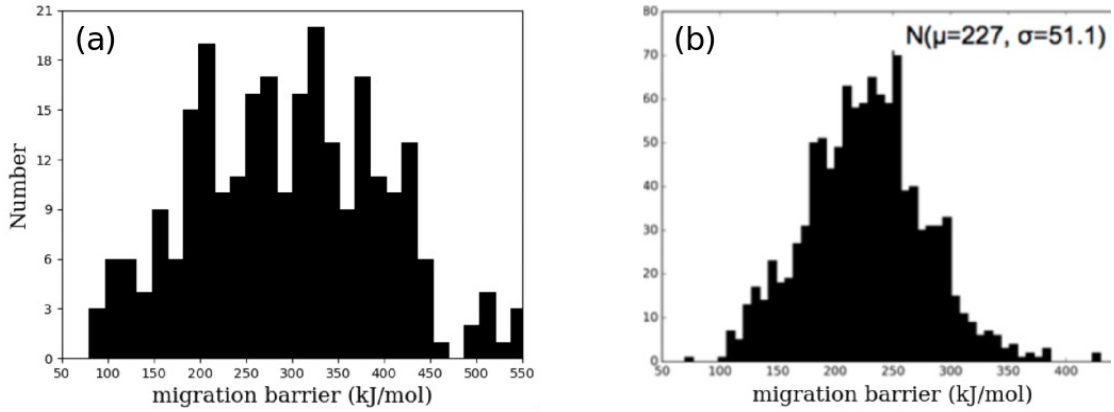

Figure 3. *Energy barrier distribution for potassium ion diffusion in a 4-layer periodic clay system with 100% potassium interlayers.* (a) ClayCG model and (b) all atom Clay-FF model[1] (reproduced with permission). The distribution of energy barriers in the ClayCG model was consistently found to be about 70 kJ/mol higher and 30% more broad than the corresponding all atom barriers. This effect is likely due to the inherent undersampling of high-energy paths during the IBI algorithm.

Both the CG and all-atom energy barriers correspond to timescales that are inaccessible for direct observation of diffusion events in MD simulations[25], but the ability of the ClayCG model to

approximate the energy barrier trends with respect to all atom ClayFF is promising for using this coarse-grain model as a probe for changes in diffusion barriers to infer the kinetics of ion exchange. Properly modeling ion diffusion near and far from the exchange front necessarily requires a model capable of simulating a large, heterogeneous interlayer, as well as overcoming finite size effects by modeling many interlayers (i.e. greater than 2), which is extremely computationally expensive in all-atom ClayFF.

For sufficiently small periodic systems, the finite size effect can dramatically impact the compressibility, and would be expected to increase the calculated barrier to ion diffusion artificially.[56] Therefore, we used the ClayCG model to determine the magnitude of the NEB barriers as a function of the number of simulated layers using periodic 2-interlayer, 4-interlayer, and 12-interlayer systems. Table 1 shows the average energy barrier for K^+ diffusion in K-illite as a function of the number of clay layers, and the energy barrier distributions determined by NEB are presented in Figure S3. Since there is essentially no observed change in the average energy barrier and variance between the 4- and 12-interlayer systems, simulating at least 4 interlayers should be sufficient to approximate an effectively infinite clay for the purposes of this study.

Table 1. Average Energy Barrier (and variance) for K^+ ion diffusion in periodic K-illite as a function of the number of interlayers. Very small systems greatly overestimate the barrier due to finite size effects. Both the ClayCG model and the all-atom model in ClayFF feature very broad energy barrier distributions.

# of Interlayers	Average Energy Barrier and variance (kJ/mol)
2	332 +/- 131
4	300 +/- 94
12	298 +/- 95

Interlayer energetics and ion migration barriers in interstratified and homostructured illite. Mixing of unlike ions in layered silicate interlayers can adopt different structures depending on the ion distributions in the interlayer of the multi-layer structure. When interlayer ions form random mixtures the phase is homostructured, and when ions are separated into distinct phase-separated layers the phase is interstratified. One advantage of our ClayCG model is the ability to model numerous clay structures with significantly reduced computational cost. In the following section we analyze the impact of homostructured vs. interstratified clay structures on the barriers to ion migration, and consequently on the kinetics of ion exchange, using ClayCG.

These systems consisted of four periodic anhydrous interlayer regions between five illite clay layers stacked in a vertical configuration. The outer layers lack counterions on the exterior basal surfaces, which is necessary to allow convergence of the simulation cell size during the shrinkwrap procedure in LAMMPS. Although redistributing these ions in the interlayers is not physically realistic, it is not expected to significantly alter the equilibrium interlayer spacing or NEB energies, because basal spacing is controlled primarily by the counterion size.

Table 2. Average energy barrier (and variance) for Cs^+ and K^+ ion diffusion in a 4-layer periodic clay system as a function of interlayer composition. Each system featured a homogenous mixture of bound Cs^+ and K^+ ions in all four interlayers. Interlayer expansion as a function of composition was very nearly linear, with an interlayer expansion of 0.071 Å under complete exchange for Cs^+.

Fraction Cs^+ in the interlayer	K^+ NEB Barrier and Variance (kJ/mol)	Cs^+ NEB Barrier and Variance (kJ/mol)	Interlayer Spacing (nm)
0	300 ± 94	321 ± 83	0.984
0.25	286 ± 83	309 ± 75	0.997
0.5	279 ± 94	295 ± 68	1.015
0.75	262 ± 84	283 ± 88	1.032
1	243 ± 74	272 ± 83	1.055

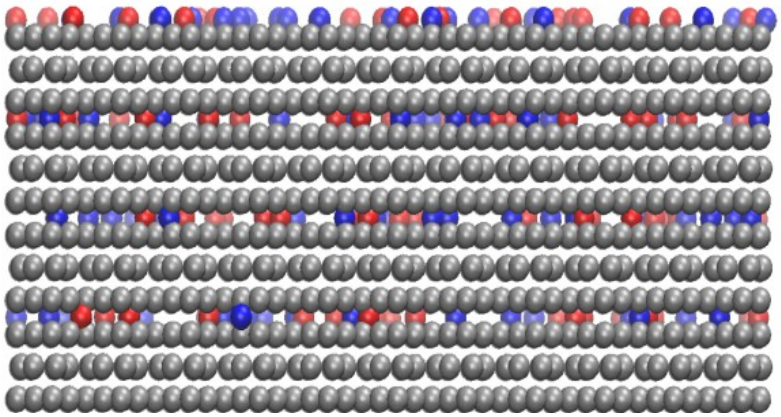

Figure 4. *Visualization of a periodic four layer homostructured clay particle in VMD.*[59] Orthographic representation showing bulk clay (gray), cesium (red), and potassium (blue) coarse-grain types. The structure is periodic in all three dimensions, with ions at the top in contact with the clay layer at the bottom of the image.

The results in Table 2 summarize the energy barriers to ion migration as a function of layer Cs^+ content for homostructured K/Cs-illites (Figure 4), in which each interlayer consisted of both Cs^+ and K^+ ions positioned randomly at counterion binding sites. As expected, both ions experience dramatically reduced energy barriers in Cs-illite compared to K-illite due to interlayer expansion,

and there is a nearly linear trend in the change in barrier height as a function of composition, consistent with prior results using atomistic models.[25] As a function of the change in equilibrium interlayer spacing, these results correspond to a decrease in the average barrier energy of approximately -71 kJ/mol per Å for Cs^+ and -78 kJ/mol per Å for K^+. This ClayCG result is similar in magnitude to the change in energy barrier found in the previous all-atom ClayFF model of -92 kJ/mol per Å for K^+,[25] on which the CG model is based.

We next consider the change in thermodynamics and kinetic barriers arising from illite clay structures with interstratification. We evaluate the excess mixing enthalpy computed as:

$$\Delta H_{mix} = H_X - f_{Cs} H_{Cs} - f_K H_K \tag{4}$$

where ΔH_{mix} is the excess enthalpy of mixing (i.e., the difference between the real and ideal enthalpy values), H_X is the computed minimum enthalpy of the clay system being simulated, f_i is the fraction of ion i in the clay system, and H_{Cs} and H_K are the enthalpies of five-layer clay containing only cesium and potassium in their interlayers, respectively (see Methods). For all of the five-layer systems investigated, each interlayer was occupied exclusively by one type of ion and did not have an exchange front. In the following tables, each five-layer system is abbreviated using the identity of the ions in its interlayers from the bottom to the top as a code. For example, the system corresponding to “Cs Cs K K” had two adjacent interlayers filled by cesium ions below two interlayers filled by potassium ions as seen in Figure 5.

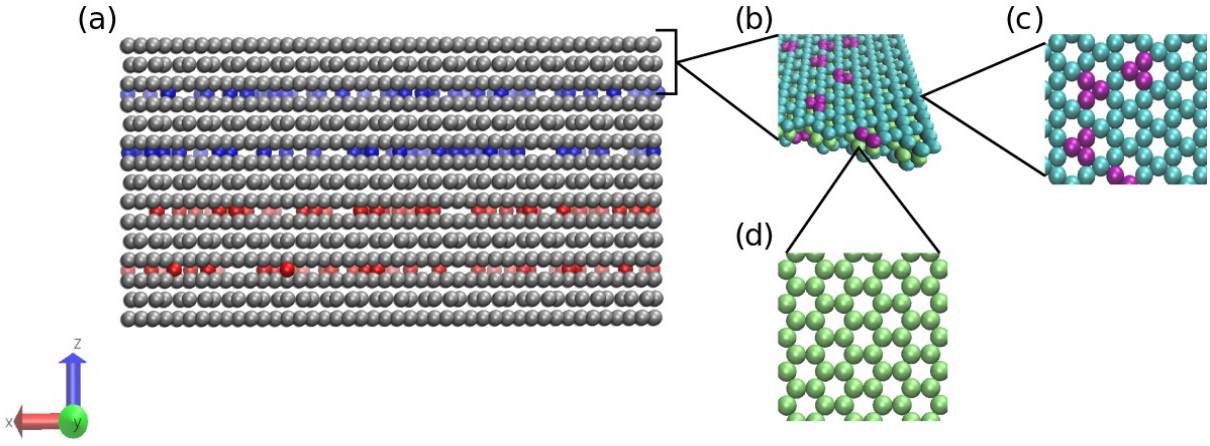

Figure 5. *Visualization of a non-periodic five layer interstratified clay system in VMD.*[57] (a) Orthographic representation showing bulk clay (gray), cesium (red), and potassium (blue) coarse-grain types; (b) top-down visualization of the three sheets in each clay layer; (c) CG centers of the tetrahedral sheet with substitutions shown in purple; (d) CG centers of the octahedral sheet.

Table 3 summarizes the trends in the layer basal spacing, energy barriers to migration, and normal stress in the z-direction on both types of ions within different interstratification arrangements. For both K^+ and Cs^+ ions, the overall trend is towards increasing normal stress (and therefore cohesion) with decreasing interlayer spacing. The presence of Cs-illite decreases z-axial stress on K-illite layers, while the presence of K^+ in the structure tends to increase z-axial stress on Cs^+ interlayers. This finding suggests that the longstanding supposition[2] that exchange on a layer increases cohesive energy in neighboring K^+ interlayers is incorrect, at least when the adjacent layer also contains anhydrous counterions. Instead, we find that exchange on one layer, regardless of its proximity to the clay interior, alters the basal spacing and cohesive energies of ions in immediately adjacent layers. As shown in Figure 6, the magnitude of this effect decreases rapidly as a function of distance from the exchanged layers, and is nearly undetectable only a few layers away from the Cs-illite/K-illite interface.

Table 3. Trends in interlayer spacing, ion diffusion energy barrier, z-axial stress, and excess mixing enthalpy versus interstratification. In general, both z-axial stress and diffusion energy barrier increase dramatically with increasing interlayer confinement. Adjacent Cs^+ interlayers are associated with a higher excess enthalpy of mixing, suggesting a thermodynamic compensation for alternation of Cs-illite and K-illite interlayers interstratified particles. For interstratified particles, NEB barriers are computed for interlayers adjacent to the of Cs-illite/K-illite interface.

Interstratification Type	**Interlayer spacing (nm)**	**NEB energy (kJ/mol)**	**z-stress (atm)**	**ΔH_{mix} (kJ/mol)**
Cs in Cs Cs Cs Cs	1.055	273	1.25	
Cs in K Cs Cs Cs	1.046	284	1.27	3.33
Cs in Cs Cs K K	1.043	289	1.29	-5.89
Cs in Cs K Cs K	1.038	291	1.35	-9.93
Cs in Cs K K K	1.041	288	1.41	-7.09
Cs in K Cs K K	1.037	286	1.38	-7.32
Cs in Cs K Cs Cs	1.049	279	1.30	0.70
K in K K K K	0.984	299	1.64	
K in Cs K K K	0.994	289	1.60	-7.09
K in Cs Cs K K	0.999	278	1.57	-5.89
K in Cs K Cs K	1.005	275	1.48	-9.93
K in K Cs Cs Cs	1.001	273	1.47	3.33
K in K Cs K K	0.990	294	1.60	-7.32

K in Cs K Cs Cs	1.001	274	1.50	0.70

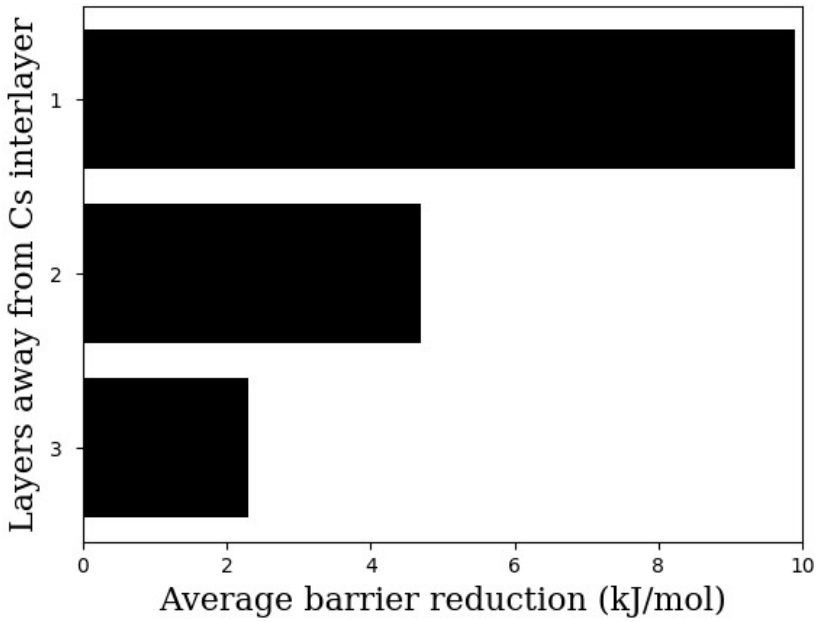

Figure 6. *Reduction in K^+ diffusion barrier in a four layer interstratified particle.* The barrier reduction to K^+ diffusion in a "Cs K K K" particle relative to bulk K-illite is shown as a function of the distance from the Cs-illite/K-illite interface.

For both types of ions, there is a clear trend of increasing energy barrier under increased confinement. In the case of only one Cs-illite layer present in bulk K-illite, it is clear from the interlayer spacing and normal stress that the cesium interlayer experiences maximal compression. To confirm this, NEB calculations were run on the displacement of a Cs^+ ion in Cs-illite in the middle of a 12-layer K-illite particle. The barrier in this case was found to be 288 kJ/mol, very similar to the 286 kJ/mol barrier for Cs^+ diffusion in the "K Cs K K" particle (Table 3), supporting the conclusion that interlayer compression and expansion in interstratified particles is a localized effect. Similarly, a K-illite layer isolated in bulk cesium relaxes to a much larger spacing.

The compensatory expansion and compression of neighboring layers may explain why the change in Cs^+ and K^+ diffusion barriers in interstratified systems is greater than the corresponding change in homostructured systems for a given interlayer spacing (summarized in Figure S4). In homostructured clays, the local interlayer spacing near a Cs^+ counterion is greater than the average interlayer spacing due to its larger atomic radius, resulting in a lower migration barrier for a given spacing. The opposite is true for K^+ counterions, which experience greater local confinement in

homostructured clays than would be expected from measuring the average interlayer spacing alone. In contrast, the compression and expansion of interlayers in interstratified clays results in a more uniform interlayer spacing, and therefore a more dramatic change in the diffusion barrier of ion migration. This effect may also be an artifact of using ClayFF as the all-atom reference model to create our CG model, as ClayFF is known to overpredict flexibility in large clay systems.

From the trends in the energy barriers to ion diffusion in K-illite interlayers adjacent to Cs-illite interlayers (Table 3), one would assume that exchange would be enhanced near cesium-dominated interlayers instead of being inhibited. That is, diffusion energy barriers in neighboring K-illite interlayers are lowered in the immediate vicinity of a Cs-illite interlayer. Experimental evidence for the Cs/K system is insufficient to confirm or refute this hypothesis, but there is some visual evidence that Cs exchanged layers occur in clumps in a K-phlogopite and are not randomly distributed, as expected from these results.[8]

Impact of the exchange front on barriers. Exchange of ions of different size leads to bending deformation of the layer structure locally, which may alter the coordination of K^+ in the vicinity of the exchange front.[58] In this case, the selectivity for and mobility of K^+ is expected to vary with the sharpness and uniformity of the front. In order to capture the effects of the sharp exchange front in anhydrous illite clay systems[7-8, 25], a series of simulations were performed in which all ions on one half of the exchanging layer were assigned to be Cs^+ and all ions on the other half were assigned to be K^+. The exchange front was modelled in a periodic, four-layer clay system that featured one completely exchanged interlayer below the exchange front and two fully unexchanged interlayers above the exchange front. Ions far from the exchange front did not have significantly altered energy barriers to diffusion compared to barriers in an interstratified particle, but K^+ ions characterized at the interface showed a slightly reduced average energy barrier compared to an interstratified clay with no exchange front barrier (273 kJ/mol vs. 278 kJ/mol). In comparison with the results of the energy barrier distribution presented in Table 2, K^+ ions near the exchange front experience approximately 20% additional barrier lowering (27 kJ/mol) with respect to the barrier in pure K-illite as compared to ions far from the front (22 kJ/mol), and ions more than approximately 2 to 3 nm from the exchange front are essentially unaffected by it.

Thermodynamic compensation for ordered interstratification. Amongst all of the non-periodic four interlayer systems studied, the system "K Cs K Cs" exhibited the greatest thermodynamic compensation for interstratification. Overall, the ΔH_{mix} trends indicate that there

is a thermodynamic driver during the exchange process to form alternating K-illite and Cs-illite layers (i.e. ordered interstratified structures).[11, 28, 59] Exchange will tend to disrupt bulk K-illite, and thermodynamic feedback will favor exchange that leads to the formation of ordered interstratification instead of regions of bulk Cs-illite. However, the thermodynamic compensation for forming ordered interstratification is quite small (at most around 10 kJ/mol), indicating that it is unlikely to be the primary cause of experimentally observed differences in the exchange rate of adjacent interlayers.[7-8]

Conclusions

We have presented a coarse-grain model of anhydrous K- and Cs-illite, ClayCG, that represents a 70-fold speedup over its parent all-atom ClayFF forcefield. Although using tabulated potentials between the oxygen coarse-grain centers may slightly improve the fidelity of modeling the ion binding sites, there is a non-negligible computational cost savings associated with using Lennard-Jones potentials as compared to splined tabulated potentials.[60] While other CG clay models have represented ion binding sites as single CG centers[39-40], the model presented here is capable of capturing physical degrees of freedom important during ion diffusion in the confined interlayer.[7, 19] By modeling all the atoms within and adjacent to the interlayer, we were able to accurately reproduce the structure of ion binding sites without significant computational overhead.

The reduction in particle density due to the coarse-grain procedure is especially helpful for nudged elastic band simulations, since the number of molecular dynamics steps necessary to reach convergence of the energy pathway is heavily dependent on system size and the number of particles surrounding the transition path. We were able to converge NEB pathways on relatively large systems, which is promising for probing the energy barriers in physical scenarios that would necessitate investigating bulk effects. Our ClayCG model qualitatively reproduced the ion diffusion energy trends as a function of interlayer separation found in ClayFF[25] and demonstrates interlayer expansion near sharp exchange fronts and near fully exchanged layers. Our model indicates a significant enthalpy of mixing associated with adjacent K- and Cs-illite interlayers in interstratified particles, which may impact exchange front propagation in adjacent interlayers. Future work will extend the coarse-graining strategy used here for ClayCG to other anhydrous and swelling clays. While the intrasheet CG bond potentials developed here for anhydrous illite will be directly portable to other clay systems, this will require introducing new intermolecular potentials for additional CG types using IBI, including water[61].

Acknowledgements. The Laboratory Directed Research and Development Program of Lawrence Berkeley National Laboratory supported KS and LNL under U.S. Department of Energy Contract No. DE-AC02-05CH11231. THG and LRP acknowledge support by the Director, Office of Science, Office of Basic Energy Sciences, of the U.S. Department of Energy under Contract No. DE-AC02-05CH11231. This research used resources of the National Energy Research Scientific Computing Center, a DOE Office of Science User Facility supported by the Office of Science of the U.S. Department of Energy under Contract No. DE-AC02-05CH11231.

References

1. Mukai, H.; Hirose, A.; Motai, S.; Kikuchi, R.; Tanoi, K.; Nakanishi, T. M.; Yaita, T.; Kogure, T. Cesium adsorption/desorption behavior of clay minerals considering actual contamination conditions in Fukushima. *Scientific reports* **2016,** *6* (October 2015), 21543.
2. Endo, S.; Kimura, S.; Takatsuji, T.; Nanasawa, K.; Imanaka, T.; Shizuma, K. Measurement of soil contamination by radionuclides due to the Fukushima Dai-ichi Nuclear Power Plant accident and associated estimated cumulative external dose estimation. *Journal of Environmental Radioactivity* **2012,** *111*, 18--27.
3. Koarashi, J.; Moriya, K.; Atarashi-Andoh, M.; Matsunaga, T.; Fujita, H.; Nagaoka, M. Retention of potentially mobile radiocesium in forest surface soils affected by the Fukushima nuclear accident. *Scientific reports* **2012,** *2*, 1005.
4. Shiozawa, S. Vertical migration of radiocesium fallout in soil in fukushima**2013,** *9784431543282*, 49--60.
5. Hashimoto, S.; Matsuura, T.; Nanko, K.; Linkov, I.; Shaw, G.; Kaneko, S. Predicted spatio-temporal dynamics of radiocesium deposited onto forests following the Fukushima nuclear accident. *Scientific Reports* **2013,** *3* (1), 2564.
6. Mukai, H.; Motai, S.; Yaita, T.; Kogure, T. Identification of the actual cesium-adsorbing materials in the contaminated Fukushima soil. *Applied Clay Science* **2016,** *121-122*, 188--193.
7. Fuller, A. J.; Shaw, S.; Ward, M. B.; Haigh, S. J.; Mosselmans, J. F. W.; Peacock, C. L.; Stackhouse, S.; Dent, A. J.; Trivedi, D.; Burke, I. T. Caesium incorporation and retention in illite interlayers. *Applied Clay Science* **2015,** *108*, 128--134.
8. Okumura, T.; Tamura, K.; Fujii, E.; Yamada, H.; Kogure, T. Direct observation of cesium at the interlayer region in phlogopite mica. *Microscopy* **2014,** *63* (1), 65--72.
9. Unterweger, M. P. Half-life measurements at the National Institute of Standards and Technology. *Applied Radiation and Isotopes* **2002,** *56* (1-2), 125--130.
10. Ishidera, T.; Kurosawa, S.; Hayashi, M.; Uchikoshi, K.; Beppu, H. Diffusion and retention behaviour of Cs in illite-added compacted montmorillonite. *Clay Minerals* **2016,** *51*, 161--172.
11. Kogure, T.; Morimoto, K.; Tamura, K.; Sato, H.; Yamagishi, A. XRD and HRTEM Evidence for Fixation of Cesium Ions in Vermiculite Clay. *Chemistry Letters* **2012,** *41* (4), 380--382.
12. Tamura, K.; Kogure, T.; Watanabe, Y.; Nagai, C.; Yamada, H. Uptake of cesium and strontium ions by artificially altered phlogopite. *Environmental Science and Technology* **2014,** *48* (10), 5808--5815.

13. Kikuchi, R.; Mukai, H.; Kuramata, C.; Kogure, T. Cs–sorption in weathered biotite from Fukushima granitic soil. *Journal of Mineralogical and Petrological Sciences* **2015,** *110* (3), 126--134.
14. Okumura, M.; Nakamura, H.; Machida, M. Mechanism of strong affinity of clay minerals to radioactive cesium: First-principles calculation study for adsorption of cesium at frayed edge sites in muscovite. *Journal of the Physical Society of Japan* **2013,** *82* (3).
15. Sawhney, B. L. Selective sorption and fixation of cations by clay minerals. A review. 1972; Vol. 20, pp 93--100.
16. Francis, C. W.; Brinkley, F. S. Preferential adsorption of cs-137 to micaceous minerals in contaminated freshwater sediment. *Nature* **1976,** *260*, 511--513.
17. Comans, R. N. J.; Hockley, D. E. Kinetics of cesium sorption on illite. *Geochimica et Cosmochimica Acta* **1992,** *56* (3), 1157--1164.
18. Lai, T.; Mortland, M. Diffusion of ions in bentonite and vermiculite. *Soil Science Society of America* **1961,** *25* (5), 353--357.
19. Liu, X. D.; Lu, X. C. A thermodynamic understanding of clay-swelling inhibition by potassium ions. *Angewandte Chemie - International Edition* **2006,** *45* (38), 6300--6303.
20. Poinssot, C.; Baeyens, B.; Bradbury, M. H. Experimental and modelling studies of caesium sorption on illite. *Geochimica et Cosmochimica Acta* **1999,** *63* (19-20), 3217--3227.
21. Tsai, S. C.; Wang, T. H.; Li, M. H.; Wei, Y. Y.; Teng, S. P. Cesium adsorption and distribution onto crushed granite under different physicochemical conditions. *Journal of Hazardous Materials* **2009,** *161* (2-3), 854--861.
22. Zaunbrecher, L. K.; Cygan, R. T.; Elliott, W. C. Molecular models of cesium and rubidium adsorption on weathered micaceous minerals. *Journal of Physical Chemistry A* **2015,** *119* (22), 5691--5700.
23. Lee, J.; Park, S. M.; Jeon, E. K.; Baek, K. Selective and irreversible adsorption mechanism of cesium on illite. 2016.
24. Nakao, A.; Thiry, Y.; Funakawa, S.; Kosaki, T. Characterization of the frayed edge site of micaceous minerals in soil clays influenced by different pedogenetic conditions in Japan and northern Thailand. *Soil Science and Plant Nutrition* **2008,** *54* (4), 479--489.
25. Pestana, L. R.; Kolluri, K.; Head-Gordon, T.; Nielsen-Lammers, L. Direct Exchange Mechanism for Interlayer Ions in Non-Swelling Clays. *Environmental Science \& Technology* **2017,** *51* (1), 393--400.
26. Comans, R. N. J.; Haller, M.; Preter, P. D. Sorption of cesium on illite: Non-equilibrium behaviour and reversibility. *Geochimica et Cosmochimica Acta* **1991,** *55* (2), 433--440.
27. Rosso, K. M.; Rustad, J. R.; Bylaska, E. J. The Cs/K exchange in muscovite interlayers: An AB initio treatment. *Clays and Clay Minerals* **2001,** *49* (6), 500--513.
28. Stixrude, L.; Peacor, D. R. First-principles study of illite – smectite and implications for clay mineral systems. *Nature* **2002,** *420*, 165--168.
29. Inoue, A. Thermodynamic Study of Na-K-Ca Exchange Reactions in vermiculite. *Clay and Clay Minerals* **1984,** *32* (4), 311--319.
30. Inoue, A.; Minato, H. Ca-K EXCHANGE REACTION AND INTERSTRATIFICATION IN MONTMORILLONITE. *Clays and Clay Minerals* **1979,** *27* (6), 393--401.
31. Marry, V.; Turq, P.; Rotenberg, B.; Jardat, M.; Dufrche, J.-F.; Marry, V.; Rotenberg, B.; Turq, P. Salt exclusion in charged porous media: a coarse-graining strategy in the case of montmorillonite clays. *Physical Chemistry Chemical Physics* **2009,** *11*, 1869.
32. Liu, C. An ion diffusion model in semi-permeable clay materials. *Environmental Science and Technology* **2007,** *41* (15), 5403--5409.

33. Sheng, N.; Boyce, M. C.; Parks, D. M.; Rutledge, G. C.; Abes, J. I.; Cohen, R. E. Multiscale micromechanical modeling of polymer/clay nanocomposites and the effective clay particle. *Polymer* **2004,** *45* (2), 487--506.
34. Gelineau, P.; Stepie. Elastic properties prediction of nano-clay reinforced polymer using multi-scale modeling based on a multi-scale characterization. *Mechanics of Materials* **2015,** *89,* 12--22.
35. Ebrahimi, D.; Pellenq, R. J. M.; Whittle, A. J. Mesoscale simulation of clay aggregate formation and mechanical properties. *Granular Matter* **2016,** *18* (3).
36. Ebrahimi, D.; Whittle, A. J.; Pellenq, R. J. M. Mesoscale properties of clay aggregates from potential of mean force representation of interactions between nanoplatelets. *J. Chem. Phys.* **2014,** *140* (15), 154309.
37. Katti, D. R.; Matar, M. I.; Katti, K. S.; Amarasinghe, P. M. Multiscale modeling of swelling clays: A computational and experimental approach. *KSCE Journal of Civil Engineering* **2009,** *13* (4), 243--255.
38. Delhorme, M.; Labbez, C.; Caillet, C. l.; Thomas, F. Acid-base properties of 2:1 clays. I. modeling the role of electrostatics. *Langmuir* **2010,** *26* (12), 9240--9249.
39. Suter, J. L.; Groen, D.; Coveney, P. V. Mechanism of Exfoliation and Prediction of Materials Properties of Clay-Polymer Nanocomposites from Multiscale Modeling. *Nano Letters* **2015,** *15* (12), 8108--8113.
40. Suter, J. L.; Groen, D.; Coveney, P. V. Chemically specifi C multiscale modeling of clay-polymer nanocomposites reveals intercalation dynamics, tactoid self-assembly and emergent materials properties. *Advanced Materials* **2015,** *27* (6), 966--984.
41. Plimpton, S. Fast Parallel Algorithms for Short-Range Molecular Dynamics. 1995; Vol. 117, pp 1--19.
42. Cygan, R. T.; Liang, J.-J.; Kalinichev, A. G. Molecular Models of Hydroxide, Oxyhydroxide, and Clay Phases and the Development of a General Force Field. *The Journal of Physical Chemistry B* **2004,** *108* (4), 1255--1266.
43. Bourg, I. C.; Sposito, G. Connecting the molecular scale to the continuum scale for diffusion processes in smectite-rich porous media. *Environmental Science and Technology* **2010,** *44* (6), 2085--2091.
44. Ferrage, E.; Sakharov, B. A.; Michot, L. J.; Delville, A.; Bauer, A.; Lanson, B.; Grangeon, S.; Frapper, G.; Jimnez-Ruiz, M.; Cuello, G. J. Hydration properties and interlayer organization of water and ions in synthetic na-smectite with tetrahedral layer charge. Part 2. Toward a precise coupling between molecular simulations and diffraction data. *Journal of Physical Chemistry C* **2011,** *115* (5), 1867--1881.
45. Marry, V.; Dubois, E.; Malikova, N.; Durand-Vidal, S.; Longeville, S.; Breu, J. Water dynamics in hectorite clays: Infuence of temperature studied by coupling neutron spin echo and molecular dynamics. *Environmental Science and Technology* **2011,** *45* (7), 2850--2855.
46. Henkelman, G.; Jnsson, H. Improved tangent estimate in the nudged elastic band method for finding minimum energy paths and saddle points. *Journal of Chemical Physics* **2000,** *113* (22), 9978--9985.
47. Henkelman, G.; Uberuaga, B. P.; Jnsson, H. Climbing image nudged elastic band method for finding saddle points and minimum energy paths. *Journal of Chemical Physics* **2000,** *113* (22), 9901--9904.
48. Maras, E.; Trushin, O.; Stukowski, A.; Ala-Nissila, T.; Jnsson, H. Global transition path search for dislocation formation in Ge on Si(001). *Computer Physics Communications* **2016,** *205*, 13--21.

49. Hardy, D. J.; Stone, J. E.; Schulten, K. Multilevel summation of electrostatic potentials using graphics processing units. *Parallel Computing* **2009,** *35* (3), 164--177.
50. Hardy, D. J.; Wu, Z.; Phillips, J. C.; Stone, J. E.; Skeel, R. D.; Schulten, K. Multilevel summation method for electrostatic force evaluation. *Journal of Chemical Theory and Computation* **2015,** *11* (2), 766--779.
51. Henderson, R. L. A uniqueness theorem for fluid pair correlation functions. *Physics Letters A* **1974,** *49* (3), 197--198.
52. Schommers, W. A pair potential for liquid rubidium from the pair correlation function. *Physics Letters A* **1973,** *432* (2), 157--158.
53. Perakis, F.; Marco, L. D.; Shalit, A.; Tang, F.; Kann, Z. R.; Khne, T. D.; Torre, R.; Bonn, M.; Nagata, Y. Vibrational Spectroscopy and Dynamics of Water. 2016; Vol. 116, pp 7590--7607.
54. Johnson, M. E.; Head-Gordon, T.; Louis, A. A. Representability problems for coarse-grained water potentials. *Journal of Chemical Physics* **2007,** *126* (14).
55. Louis, A. A. Beware of density dependent pair potentials. *Journal Of Physics-Condensed Matter* **2002,** *14* (40), 9187--9206.
56. Salacuse, J.; Denton, a.; Egelstaff, P. Finite-size effects in molecular dynamics simulations: Static structure factor and compressibility. I. Theoretical method. *Physical Review E* **1996,** *53* (3), 2382--2389.
57. Humphrey, W.; Dalke, A.; Schulten, K. VMD: Visual molecular dynamics. *Journal of Molecular Graphics* **1996,** *14* (1), 33--38.
58. REICHENBACHT, H. G. V.; RICH, C. I. Potassium release from muscovite as influenced by particle size. *Clays and Clay Minerals* **1969,** *17* (1), 23--29.
59. Nadeau, P. H.; Wilson, M. J.; McHardy, W. J.; Tait, J. M. Interstratified clays as fundamental particles. *Science (New York, N.Y.)* **1984,** *225* (4665), 923--925.
60. Wolff, D.; Rudd, W. G. Tabulated potentials in molecular dynamics simulations. *Computer Physics Communications* **1999,** *120* (1), 20--32.
61. Johnson, M. E.; Head-Gordon, T. Assessing thermodynamic-dynamic relationships for waterlike liquids. *J Chem Phys* **2009,** *130* (21), 214510.